Targeted degradation of IKZF2 for cancer immunotherapy

Jonathan Solomon (jonathan.solomon@novartis.com)
Novartis Institutes for BioMedical Research https://orcid.org/0000-0002-4588-2751

Simone Bonazzi
Novartis Institutes for Biomedical Research

Eva d'Hennezel
Novartis Institutes for Biomedical Research

Rohan Beckwith
Novartis Institutes for Biomedical Research

Lei Xu
Novartis Institutes for Biomedical Research

Aleem Fazal
Novartis https://orcid.org/0000-0003-0643-0477

Anna Magracheva
Novartis Institutes for Biomedical Research

Radha Ramesh
Novartis Institutes for Biomedical Research

Artiom Cernijenko
Novartis Institutes for Biomedical Research

Brandon Antonakos
Novartis Institutes for Biomedical Research

Hyo-eun Bhang
Novartis Institutes for Biomedical Research

Roxana Garcia Caro
Novartis Institutes for Biomedical Research

Jennifer Cobb
Novartis Institutes for Biomedical Research

Elizabeth Ornelas
Novartis Institutes for Biomedical Research

Xiaolei Ma
Novartis Institutes for Biomedical Research

Charles Wartchow
Novartis Institutes for Biomedical Research

Matt Clifton

Novartis Institutes for Biomedical Research

Ry Forseth
Novartis Institutes for Biomedical Research

Bethany Fortnam
Novartis Institutes for Biomedical Research

Hongbo Lu
Novartis Institutes for Biomedical Research

Alfredo Csibi
Novartis Institutes for Biomedical Research

Jennifer Tullai
Novartis Institutes for Biomedical Research

Seth Carbonneau
Novartis Institutes for BioMedical Reserarch

Noel Thomsen
Novartis Institutes for Biomedical Research

Jay Larrow
Novartis Institutes for Biomedical Research

Barbara Chie-Leon
Novartis Institutes for Biomedical Research

Dominik Hainzl
Novartis Institutes for Biomedical Research

Yi Gu
Novartis Institutes for Biomedical Research

Darlene Lu
Novartis Institutes for Biomedical Research

Matthew Meyer
Novartis Institutes for Biomedical Research

Dylan Alexander
Novartis Institutes for Biomedical Research

Jacqueline Kinyamu-Akunda
Novartis Institutes for Biomedical Research

Catherine Sabatos-Peyton
Novartis Institutes for Biomedical Research

Natalie Dales
Novartis Institutes for Biomedical Research

Frederic Zecri
Novartis Institutes for Biomedical Research

Rishi Jain
Novartis Institutes for Biomedical Research

Janine Shulok
Novartis Institutes for Biomedical Research
Y. Karen Wang
Novartis Institutes for Biomedical Research
Karin Briner
Novartis Institutes for Biomedical Research
Jeffrey Porter
Novartis Institutes for Biomedical Research
John Tallarico
Novartis Institutes for Biomedical Research https://orcid.org/0000-0002-8040-8422
Jeffrey Engelman
Novartis Institutes for Biomedical Research
Glenn Dranoff
Novartis Institutes for Biomedical Research
Jay Bradner
Novartis (United States) https://orcid.org/0000-0002-2718-4415
Michael Visser
Novartis Institutes for Biomedical Research

Biological Sciences - Article

Keywords:

Posted Date: April 8th, 2022

DOI: https://doi.org/10.21203/rs.3.rs-1531006/v1

Abstract

Growing malignant tumors must evade destruction by the immune system, a hurdle some malignancies overcome by attracting immune-suppressive regulatory T-cells (Tregs)1. The IKZF2 (Helios) transcription factor plays a crucial role in maintaining function and stability of Tregs, and IKZF2 deficiency enhances immune responses to tumors in mice2, suggesting IKZF2 may be an attractive target for cancer immunotherapy. Here we describe the discovery and characterization of DKY709, the first molecular glue degrader of IKZF2/4 which spares IKZF1/3. DKY709 was identified through a recruitment-guided medicinal chemistry campaign that redirected the degradation selectivity of CRBN binders towards IKZF2. The IKZF transcription factor selectivity of DKY709 was rationalized by the X-ray structure of the CRBN-DKY709-IKZF2(ZF2) ternary complex. Upon exposure to DKY709, human Tregs showed reduced suppressive activity and exhausted T-effector cells recovered IFNγ production. In vivo, oral treatment with DKY709 drove a rapid and sustained degradation of IKZF2 including in humans and led to delayed tumor growth in mice with humanized immune systems and enhanced immunization responses in monkeys. DKY709 is a first-in-class, potent and selective oral IKZF2/4 degrader currently being investigated in a phase 1 clinical trial as an immune-enhancing agent for cancer immunotherapy.

Introduction

Tumors evade destruction by the immune system by deploying multiple mechanisms to dampen anti-tumor immune responses[3]. These include exploiting the intrinsic negative feedback mechanisms of the immune system, such as inhibitory cells and inhibitory receptors (e.g. PD-1 and CTLA-4)[4]. Cancer immunotherapies aim to reverse these immuno-evasive strategies and restore immune effector functions in the tumor[5]. Recently developed therapies using PD-1 or CTLA4-blocking antibodies benefit only a minority of eligible patients[1]. Hence, metastatic cancer remains largely incurable and further advances in cancer immunotherapies are needed.

FOXP3+ regulatory T cells (Treg) cells are critical for the maintenance of immunological self-tolerance and immune system homeostasis[6], but also limit anti-tumor immune response by suppressing the activation and expansion of tumor-specific effector T (Teff) cells[1,7]. Chronic exposure of Teff cells to the tumor can also lead to reduced effector functions and to the upregulation of immune inhibitory receptors like PD-1[1]. Therapies that more effectively target Treg and dysfunctional Teff cells in the tumor may extend the benefit of immunotherapy to more patients with cancer.

IKZF2 (Helios), a member of the Ikaros transcription factor family[8,9], is primarily expressed in a majority of Treg cells and some T cell and lymphocyte subsets[10,11]. IKZF2-deficient mice show decreased lineage stability of Treg cells, which promotes the secretion of pro-inflammatory cytokines[12] and leads to enhanced anti-tumor immune response in mouse syngeneic tumor models[2]. Recent evidence has further implicated IKZF2 in dysfunctional Teff cells in tumors[13,14]. Germline mutations of *IKZF2* in humans have also recently been associated with chronic T cell activation and increased production of pro-inflammatory

cytokines both in effector and regulatory T cells[15,16]. Taken together, these data suggest that degradation of IKZF2 in Tregs and other T cells may enhance the anti-tumor immune response, making IKZF2 an attractive target for cancer immunotherapy.

Zinc finger transcription factors such as IKZF2 are challenging drug targets because they are mostly unstructured and lack ligandable sites[17]. However, the immunomodulatory drugs (IMiDs) pomalidomide (**1**) and lenalidomide (**2**) (Extended Data Fig. 1a), induce degradation of the closely related IKZF1 and IKZF3 transcription factors[18,19]. IMiDs do not bind IKZF1/3 on their own but first bind the CRBN E3 ligase[20,21,22], generating a composite protein-small molecule surface that can recruit neo-substrates[23]. IKZF1 and 3 recruited to IMiD-bound CRBN are then tagged with poly-ubiquitin leading to their degradation by the proteasome[18,19]. In this way CRBN molecular glue degraders can overcome the obstacles to drugging a transcription factor. CRBN glue degraders can be structurally modified to target new proteins[24,25] such as GSPT1, ZMYM2 and ZBTB16[26,27,28] and therefore represent an emerging therapeutic modality[29] which could also be applied to IKZF2.

In this work we set out to develop a novel cancer immunotherapy targeting tumor infiltrating Tregs to enhance antitumor immunity. We describe the discovery of DKY709, a first-in-class selective CRBN glue degrader of IKZF2/4 using a new recruitment-based approach. We show that DKY709 modulated Treg and Teff cell functions *in vitro*, and enhanced immune response and delayed tumor growth *in vivo*. DKY709 has entered the clinic in a Phase 1 trial for solid tumor indications (ClinicalTrials.gov NCT03891953) and has demonstrated profound and sustained degradation of IKZF2 in human patients.

Results

Discovery of IKZF2/4 degrader DKY709

Pomalidomide (**1**) (Extended Data Fig. 1a) is a potent IKZF1 degrader (DC_{50} 10 nM, maximal percent degradation (D_{max} 84%)), but has no effect on IKZF2 protein levels up to 50 μM (Fig. 1a). However, pomalidomide (**1**) does induce a measurable interaction between IKZF2 and CRBN in cells as measured by a split enzyme recruitment assay (A_{max} 460%), an interaction only four-fold weaker than that seen with IKZF1 (A_{max} 1940%) (Fig. 1b, Extended Data Table 1). These data suggested that pomalidomide (**1**) could be a starting point for identification of molecules that more potently recruit IKZF2 to CRBN.

Pomalidomide (**1**)-bound CRBN binds to a glycine beta-hairpin in zinc finger 2 of IKZF1[18,23]. The zinc finger 2 beta-hairpin of IKZF1 and IKZF2 differ by a single amino acid (Q146 vs H141) (Extended Data Fig. 1b). To address concerns that unfavorable interactions outside of the beta hairpin might hamper IKZF2 degradation by CRBN, tagged versions of full length IKZF1, IKZF2 or IKZF2(H141Q) mutant were expressed in cells and their degradation was measured in the presence of increasing concentrations of pomalidomide (**1**) (Fig. 1a). Full length IKZF2(H141Q) was degraded as efficiently by pomalidomide (**1**) as full length IKZF1 demonstrating that the single amino acid difference in the beta hairpin is solely

responsible for the inability of pomalidomide (**1**) to degrade IKZF2 and that a compound that can accommodate the histidine in IKZF2 zinc finger 2 could be an IKZF2 degrader.

Initial SAR exploration identified compound (**3**) as a good starting point for the MedChem effort (Fig. 1c). Addition of a cyclopropyl residue at C(5) on the isolindolinone core showed substantial reduction in IKZF1 recruitment compared to pomalidomide (**1**) (A_{max} 600% vs 1940%), while maintaining a similar level of IKZF2 recruitment (A_{max} 340% vs 460%). This suggested that substitution at C(5) may be preferred to achieve IKZF2 selectivity and supported the feasibility of independently modulating the recruitment of the two proteins to CRBN. Compound (**3**) did not degrade either IKZF1 or IKZF2 in the engineered cellular degradation assay. A phenyl ring at C(5) (**4**) recruited IKZF2 more strongly to CRBN than IKZF1 (A_{max} 520% vs 290%) and a cyclohexyl ring (**5**) slightly increased IKZF2 recruitment (A_{max} 550%), but with no signs of IKZF2 degradation. Replacement of the cyclohexyl group with a piperidine (**6**) led to a substantial increase in IKZF2 recruitment (A_{max} 1050%, 400% recruitment at 1.26 μM) that translated into a weak degradation of IKZF2 (D_{max} 29%, DC_{50} > 50 μM). The addition of the basic amine also improved compound solubility compared to the previously described derivatives, but strongly decreased its permeability (Extended Data Table 1). Subsequent SAR optimization focused on improving the level of IKZF2 degradation while optimizing the physicochemical properties of the compound. The addition of a benzyl group to the piperidine gave compound (**7**), hereafter referred to as DKY709. This modification strongly improved recruitment of IKZF2 (A_{max} 1350%, 400% recruitment at 0.009 μM) that translated into strong IKZF2 degradation (D_{max} 53%, DC_{50} 4 nM). DKY709 recruited IKZF1 to CRBN (A_{max} 550%, 400% recruitment at 0.28 μM), but had no effect on IKZF1 degradation in the cellular assay up to 50 μM (Fig. 1c). DKY709 showed improved permeability compared to compound (**6**) and maintained good solubility (Extended Data Table 1). As expected, DKY709 showed strong CRBN binding in biochemical and cellular assays (Extended Data Table 1) and no degradation of IKZF2 in CRBN KO cells (Fig. 1d) confirming IKZF2 downregulation through a CRBN-mediated mechanism. Degradation of endogenous IKZF2 was assessed in the Jurkat human T-cell cancer cell line which expresses both IKZF2 and IKZF1. Treatment with DKY709 for 16-20 hours led to dose-dependent and selective degradation of IKZF2 (D_{max} 69%, DC_{50} 11 nM) with no effect on IKZF1 (Fig. 1e).

Selectivity of CRBN glue degrader DKY709

The broader cellular selectivity of DKY709 was evaluated by quantitative proteomics. Jurkat cells were treated with 2.5 μM of DKY709 for 16 hours. Among the 8656 quantified proteins, only IKZF2 was significantly downregulated (Fig. 1f). These data also confirmed that other Ikaros family members, IKZF1 and IKZF3, as well as the more distantly related IKZF5 were not downregulated by DKY709. IKZF4 and SALL4 could not be detected in Jurkat cells.

Engineered cellular assays were used to assess the selectivity of DKY709 and its precursors for other important β-hairpin containing targets. IKZF4, whose zinc finger 2 beta hairpin sequence is identical to

IKZF2 (Extended Data Fig. 1b) was weakly degraded by DKY709 (DC_{50} 5 nM, D_{max} 21%) (Extended Data Fig. 1c). DKY709 degraded the SALL4 zinc finger transcription factor (D_{max} 55%, DC_{50} 2 nM (Prolabel), D_{max} 88%, DC_{50} 13 nM (HiBit)) (Extended Data Fig. 1d and Extended Data Table 1). SALL4 is not expressed in differentiated immune cells[30], but SALL4 reduction has been linked to IMID-induced teratogenicity[31,32]. The translation termination factor GSPT1, an important anti-target because its reduction blocks new protein synthesis[33], was not degraded by DKY709 up to 50 μM (Extended Data Fig. 1e and Extended Data Table 1).

Biophysical and structural characterization

The binding of recombinant IKZF2 zinc-fingers to the DDB1:CRBN:DKY709 complex was first explored using Surface Plasmon Resonance (SPR) (Fig. 2a, Extended Data Fig. 2a,b). The affinities of IKZF2 truncated proteins containing ZF2, ZF2-3, and ZF1-4 were 4.2 ± 1.6 μM, 0.19 ± 0.01 μM and 0.56 ± 0.06 μM, respectively (Fig. 2b). While ZF2 alone bound to DDB1:CRBN:DKY709, ZF2-3 bound with 22-fold greater affinity, suggesting that ZF3 also contributes to binding. The binding affinity of ZF2-3 and the longer ZF1-4 constructs are similar, indicating that ZF2-3 is the minimal binding component of IKZF2 that interacts with CRBN in the presence of DKY709.

The X-ray structure of CRBNΔ40/DDB1ΔBPB bound to IKZF2(ZF2) in the presence of DKY709 was determined to 3.15 Å resolution (Extended Data Fig. 2c). Unlike the recently published CRBN:IKZF2(ZF2) structure[34], CRBN was bound to DKY709:IKZF2(ZF2) in the “open” conformation similarly to the CRBN-IKZF1(ZF2) complex[25] where the IMiD-binding domain (IBD) rotates ~45 degrees relative to the rest of the complex (Extended Data Fig. 2c). The structure resembles previously described CRBN-DDB1 complexes bound to C2H2 zinc-finger transcription factors where the characteristic β-hairpin structural degron is observed and G146 accommodates the phthalimide moiety of the IMiD[23]. The protonated piperidine nitrogen of DKY709 engages CRBN(E377) by a salt bridge while the benzyl substituent in DKY709 is solvent exposed (Fig. 2c). IKZF2 and IKZF1 differ by a single amino acid (IKZF2(H141) vs IKZF1(Q146)) within the structurally resolved region. In IKZF2, H141 makes a CH-π interaction with the bulky piperidine in DKY709. In IKZF1, Q146 does not allow for the same CH-π interaction and the sidechain clashes with DKY709, conferring selectivity against IKZF1 (Fig. 2d).

Impact of DKY709 on T cells *in vitro*

Transcription of Interleukin-2 (IL-2) can be repressed by both IKZF2 and IKZF1[35]. DKY709 treatment of Jurkat T cells stimulated with phyto-hemagglutinin (PHA) led to a dose-dependent increase in IL-2 concentration in the supernatant (Extended Data Fig. 3a). This effect was comparable in magnitude to the increase in IL-2 induced by pomalidomide (**1**)-driven degradation of IKZF1/3. These data show that DKY709, which degrades only IKZF2 in Jurkat cells (Fig. 1e,f), can potently modulate a known IKZF2 transcriptional target *in vitro*.

We next examined the impact of DKY709 on primary human Treg phenotype and function *in vitro*. A dose-dependent degradation of IKZF2, and not IKZF1, was observed in human primary CD25-enriched T cells upon treatment with DKY709 (D_{max} 89%, DC_{50} 11 nM) (Fig. 3a). Degradation of endogenous IKZF4 was not assessed in human cells due to lack of adequate reagents. Treg cells stimulated and expanded *in vitro* in the presence of DKY709 showed over 90% reduction in IKZF2 protein levels (MFI) (Fig. 3b) and a decreased capacity to suppress Teff cells proliferation (Fig. 3c). These data demonstrated the ability of DKY709 to induce modulation of Treg cell phenotype and function *in vitro* (Fig. 3c).

We additionally explored the impact of DKY709 on the functions of effector T cells. T cell dysfunction was induced *in vitro* in primary human PBMCs by repeated T-cell receptor (TCR) stimulation. T cells exhausted in the presence of DKY709 displayed a dose-proportional reduction in IKZF2+ cells (Fig. 3d) and an increase in IFNg-expressing, IKZF2+ CD4 and CD8 T cells (Fig. 3e and Extended Data Fig. 3b). These results show for the first time a functional impact of IKZF2/4 reduction in circumventing Teff exhaustion and highlight de-repression of IFNg production as a biomarker of IKZF2/4 degradation in primary T cells.

DKY709 leads to immune modulation and reduced tumor growth *in vivo*

DKY709 displayed favourable PK properties in mice and monkeys, with rapid absorption, good bioavailability and moderate clearance (Extended Data Fig. 4a). IMiDs lack activity in rodents[24], and we verified that DKY709 degrades IKZF2 in human, non-human primate and rabbit cells, but not in other species tested, including mice (Extended Data Fig. 4b,c). Therefore, the impact of DKY709 on immune modulation and tumor growth *in vivo* was measured in mice with humanized (hematopoietic stem-cell derived) immune systems. These mice were implanted with MDA-MB231 (breast cancer) xenografts and dosed with DKY709 at 100 mg/kg once daily (Fig. 4a). This treatment resulted in robust IKZF2 degradation in both tumor and peripheral blood Tregs (Fig. 4b). Single agent DKY709 treatment led to reduced tumor growth, comparable to treatment with the anti-PD1 antibody PDR001 as a single agent (Fig. 4c, $p<0.05$ versus vehicle), although no additional efficacy was detected in the combination of DKY709 with PDR001. DKY709 treatment also led to reduced expression of the key biomarkers of fitness, CD25 (IL2Rα) and FOXP3, in the tumor-infiltrating Tregs (Fig. 4d). These results are consistent with the hypothesis that IKZF2/4 degradation leads to the destabilization of Tregs cells in the tumor and subsequently increases tumor rejection.

Degradation of IKZF2 in circulating Tregs was detected in cynomolgus monkeys after a single oral dose of DKY709. Maximum degradation (~90% at 1 mg/kg) occurred 24 hours post-dose and partial degradation was seen with a dose as low as 0.01 mg/kg (Fig. 4e). Immune modulation downstream of daily oral DKY709-treatment was studied using a protocol of monkey immunization with experimental antigens (KLH/squalene) (Fig. 4f). Sustained degradation of IKZF2 was observed (Fig. 4g), which was associated with a measurable increase in KI67+, proliferating T cells in the PBMCs of immunized animals (Fig. 4h), reflecting a potentiation of the T cell response to the immunization protocol.

Based on positive preclinical data and favorable development properties, DKY709 entered the clinic for solid tumors indications (ClinicalTrials.gov NCT03891953). Steady-state plasma concentration-time profiles from two patients treated with 20 mg DKY709 orally once daily revealed that DKY709 concentrations remained above 50 ng/mL (Fig. 4i). This threshold, after conversion to an equivalent unbound concentration, corresponded to the concentrations leading to about 80% IKZF2 degradation *in vitro* in human PBMC (Fig. 4i and 3a). At this dose, we observed a rapid and profound decrease of IKZF2 in peripheral FOXP3+ T cells (Fig. 4j), with over 80% reduction in IKZF2-positive Tregs within 24 hours after the first dose and reaching over 90% degradation at steady-state (4-6 weeks) of daily treatment (Fig. 4j). These results confirm DKY709 is a potent degrader of IKZF2 in humans able to sustain high IKZF2 degradation with once daily dosing.

Discussion

The medicinal chemistry effort that identified DKY709 was guided by an IKZF2-CRBN recruitment assay rather than only measuring degradation. This led to the discovery of a high recruitment threshold required for both IKZF1 and IKZF2 degradation. Measuring target-CRBN recruitment allowed us to identify diverse starting points and progress chemical matter before degradation was detectable. The recruitment threshold rationalizes how CRBN glue degraders can achieve degradation selectivity while binding to a similar beta-hairpin structural degron present in many proteins. In summary, while measuring degradation is essential to assess potency and selectivity, we propose that monitoring target-CRBN recruitment is an improved strategy to identify and develop new CRBN glue degraders. CRBN glue degraders expand the druggable proteome to include challenging targets such as transcription factors. The recruitment-guided development of DKY709 demonstrates the ability to redefine the selectivity of CRBN glue degraders, enhancing the attractiveness of this rapidly growing modality for drug discovery.

The structural model explains how DKY709 accommodates the histidine in IKZF2(ZF2) and sterically interferes with the glutamine in IKZF1(ZF2), thus reversing the IKZF degradation selectivity of initial IMiD molecules. The DKY709 molecular glue interaction is also mediated by a series of hydrophobic and hydrogen bond interactions between IKZF2(ZF2) and the CRBN IMiD binding domain (IBD) (Extended Data Fig. 2d). However, SPR studies demonstrated that ZF3 also contributes to CRBN binding, suggesting that interactions exist beyond those captured in the structural model which remains to be elucidated.

By degrading IKZF2/4 while sparing IKZF1/3, DKY709 presents a unique opportunity to target Treg-intrinsic biology in the clinic. IKZF4 has also been shown to play a key role in supporting Treg stability and function[36,37], suggesting that degradation of endogenous IKZF4 reinforces the biological impact of IKZF2 degradation. However, IKZF1 and 3 are broadly expressed in the developing and differentiated immune system and their degradation causes pleiotropic effects[9]. Our studies with DKY709 extend previous work using IMiD analogs capable of degrading IKZF2/4 along with IKZF1/3, which have the potential for confounding effects derived from co-degradation of IKZF1 and IKZF3[34]. In addition to effects in Tregs, this work supports a functional role for IKZF2/4 on Teff cell dysfunction, validating several published reports describing the expression of IKZF2 in dysfunctional Teff cells states[13,14,38].

Together, the impact of DKY709 on both Treg and Teff cell biology highlights IKZF2/4 as a unique target opportunity to enhance anti-tumor T cell-mediated immunity. For this reason, DKY709 is currently being evaluated in a first-in-human phase 1 clinical trial in solid tumor indications (ClinicalTrials.gov NCT03891953).

Declarations

Acknowledgments:

The authors thank many Novartis colleagues whose efforts supported this work: Rob Maher, Shaojian An and John Reece-Hoyes for vector construction; Fangmin Xu for seminal proteomics studies and Tomas Rejtar for proteomics informatics expertise; Ulrich Hassipien, Holger Schlingensiepen, Christina Hebach, Erin Nolin, Dojna Shkova, Zhao Kang for enabling compound characterization. Dana Walker, William Kluwe and Fang Yang for Cynomolgus monkey study support and analysis; Eunice Kwak, Christopher Straub, Lisa Kattenhorn and Tanya Mulvey for supporting the DKY709 clinical trial; and Eunice Kwak, Viktor Hornak, Dennis Buckley and William Forrester for careful reading and editing of this manuscript. The authors also thank and acknowledge the external collaborators at Aurigene for compounds synthesis and the external collaborators at Navigate for analysis of the clinical trial samples. X-ray data was collected at the Advanced Light Source, a Department of Energy Office of Science User Facility under Contract No. DE-AC02-05CH11231.

Author Contributions:

A.F., R.E.J.B., S.B., A.C., N.M.T., J.L. designed, synthesized and/or characterized the reported compounds. L.X, J.T., S.C. developed and performed cellular assays to support compound characterization. R.G.C., J.S.C. conducted expression proteomics experiments. X.M, E.O., B.C.-L., M.C.C, C.A.W. supported and performed protein biophysics and X-ray crystallography. E.D., A.C., A.M., R.R., B.H.F., H.L. developed and performed *in vitro* immune cell assays. B.A., H.C.B. designed and performed *in vivo* mouse xenograft experiments. R.R.F., D.H. were responsible for pharmacokinetic studies. Y.G. and D.L. compiled clinical data. J.M.S., R.E.J.B. conceived the project. S.B., E.D., M.V., J.M.S, R.E.J.B. led the project. S.B., E.D., J.M.S wrote and edited the manuscript. M.J.M., D.A., J. K.-A., C.A.S.-P., N.A.D., F.J.Z., J.S., Y.K.W., K.B., J.A.P, J.A.T, J.A.E., G.D., J.E.B. contributed with intellectual and strategic input.

Competing Financial Interests: All authors are employees of Novartis or were at the time of this study.

References

1. Sharma, P., Hu-Lieskovan, S., Wargo, J. A. & Ribas, A. Primary, Adaptive, and Acquired Resistance to Cancer Immunotherapy. *Cell* vol. 168 707–723 (2017).

2. Nakagawa, H. *et al.* Instability of Helios-deficient Tregs is associated with conversion to a T-effector phenotype and enhanced antitumor immunity. *Proceedings of the National Academy of Sciences of the United States of America* **113**, 6248–6253 (2016).

3. Hanahan, D. & Weinberg, R. A. Hallmarks of cancer: The next generation. *Cell* vol. 144 646–674 (2011).

4. Pardoll, D. M. The blockade of immune checkpoints in cancer immunotherapy. *Nature Reviews Cancer* vol. 12 252–264 (2012).

5. Zhang, Y. & Zhang, Z. The history and advances in cancer immunotherapy: understanding the characteristics of tumor-infiltrating immune cells and their therapeutic implications. *Cellular and Molecular Immunology* vol. 17 807–821 (2020).

6. Sakaguchi, S. *et al.* Annual Review of Immunology Regulatory T Cells and Human Disease. (2020) doi:10.1146/annurev-immunol-042718.

7. Nishikawa, H. & Sakaguchi, S. Regulatory T cells in cancer immunotherapy. *Current Opinion in Immunology* vol. 27 1–7 (2014).

8. John, L. B. & Ward, A. C. The Ikaros gene family: Transcriptional regulators of hematopoiesis and immunity. *Molecular Immunology* vol. 48 1272–1278 (2011).

9. Read, K. A., Jones, D. M., Freud, A. G. & Oestreich, K. J. Established and emergent roles for Ikaros transcription factors in lymphoid cell development and function. *Immunological Reviews* vol. 300 82–99 (2021).

10. Cai, Q., Dierich, A., Oulad-Abdelghani, M., Chan, S. & Kastner, P. Helios Deficiency Has Minimal Impact on T Cell Development and Function. *The Journal of Immunology* **183**, 2303–2311 (2009).

11. Thornton, A. M. *et al.* Expression of Helios, an Ikaros Transcription Factor Family Member, Differentiates Thymic-Derived from Peripherally Induced Foxp3 + T Regulatory Cells . *The Journal of Immunology* **184**, 3433–3441 (2010).

12. Kim, H.-J. *et al.* Stable inhibitory activity of regulatory T cells requires the transcription factor Helios. *Science (New York, N.Y.)* **350**, 334–9 (2015).

13. Mognol, G. P. *et al.* Exhaustion-associated regulatory regions in CD8+ tumor-infiltrating T cells. *Proceedings of the National Academy of Sciences of the United States of America* **114**, E2776–E2785 (2017).

14. Singer, M. *et al.* A Distinct Gene Module for Dysfunction Uncoupled from Activation in Tumor-Infiltrating T Cells. *Cell* **166**, 1500-1511.e9 (2016).

15. Hetemäki, I. *et al. Loss-of-function mutation in IKZF2 leads to immunodeficiency with dysregulated germinal center reactions and reduction of MAIT cells*. *Sci. Immunol* vol. 6 https://www.science.org (2021).

16. Shahin, T. *et al.* Identification of Germline Monoallelic Mutations in IKZF2 in Patients with Immune Dysregulation. (2022) doi:10.1182/bloodadvances.2021006367/1854669/bloodadvances.2021006367.pdf.

17. Dang, C. v., Reddy, E. P., Shokat, K. M. & Soucek, L. Drugging the “undruggable” cancer targets. *Nature Reviews Cancer* vol. 17 502–508 (2017).

18. Krönke, J. *et al.* Lenalidomide causes selective degradation of IKZF1 and IKZF3 in multiple myeloma cells. *Science* **343**, 301–305 (2014).

19. Lu, G. *et al.* The myeloma drug lenalidomide promotes the cereblon-dependent destruction of Ikaros proteins. *Science (New York, N.Y.)* **343**, 305–9 (2014).

20. Ito, T. *et al.* Identification of a primary target of thalidomide teratogenicity. *Science (New York, N.Y.)* **327**, 1345–50 (2010).

21. Fischer, E. S. *et al.* Structure of the DDB1-CRBN E3 ubiquitin ligase in complex with thalidomide. *Nature* **512**, 49–53 (2014).

22. Chamberlain, P. P. *et al.* Structure of the human Cereblon-DDB1-lenalidomide complex reveals basis for responsiveness to thalidomide analogs. *Nature Structural and Molecular Biology* **21**, 803–809 (2014).

23. Petzold, G., Fischer, E. S. & Thomä, N. H. Structural basis of lenalidomide-induced CK1α degradation by the CRL4 CRBN ubiquitin ligase. *Nature* **532**, 127–130 (2016).

24. Krönke, J. *et al.* Lenalidomide induces ubiquitination and degradation of CK1α in del(5q) MDS. *Nature* **523**, 183–188 (2015).

25. Sievers, Q. L. *et al.* Defining the human C2H2 zinc finger degrome targeted by thalidomide analogs through CRBN. *Science* **362**, (2018).

26. Matyskiela, M. E. *et al.* A novel cereblon modulator recruits GSPT1 to the CRL4 CRBN ubiquitin ligase. *Nature* **535**, 252–257 (2016).

27. Renneville, A. *et al.* Avadomide Induces Degradation of ZMYM2 Fusion Oncoproteins in Hematologic Malignancies. *Cancer discovery* **2**, 250–265 (2021).

28. Matyskiela, M. E. *et al.* Cereblon Modulators Target ZBTB16 and Its Oncogenic Fusion Partners for Degradation via Distinct Structural Degrons. *ACS Chemical Biology* **15**, 3149–3158 (2020).

29. Chamberlain, P. P. *et al.* Evolution of Cereblon-Mediated Protein Degradation as a Therapeutic Modality. *ACS medicinal chemistry letters* **10**, 1592–1602 (2019).

30. Kohlhase, J. *et al.* Okihiro syndrome is caused by SALL4 mutations. *Human molecular genetics* **11**, 2979–87 (2002).

31. Matyskiela, M. E. *et al.* SALL4 mediates teratogenicity as a thalidomide-dependent cereblon substrate. *Nature Chemical Biology* **14**, 981–987 (2018).

32. Donovan, K. A. *et al.* Thalidomide promotes degradation of SALL4, a transcription factor implicated in Duane Radial Ray syndrome. *eLife* **7**, (2018).

33. Zhouravleva, G. *et al.* Termination of translation in eukaryotes is governed by two interacting polypeptide chain release factors, eRF1 and eRF3. *EMBO Journal* **14**, 4065–4072 (1995).

34. Wang, E. S. *et al.* Acute pharmacological degradation of Helios destabilizes regulatory T cells. *Nature Chemical Biology* **17**, 711–717 (2021).

35. Baine, I., Basu, S., Ames, R., Sellers, R. S. & Macian, F. Helios Induces Epigenetic Silencing of Il2 Gene Expression in Regulatory T Cells . *The Journal of Immunology* **190**, 1008–1016 (2013).

36. Gokhale, A. S., Gangaplara, A., Lopez-Occasio, M., Thornton, A. M. & Shevach, E. M. Selective deletion of Eos (Ikzf4) in T-regulatory cells leads to loss of suppressive function and development of systemic autoimmunity. *Journal of Autoimmunity* **105**, (2019).

37. Pan, F. *et al.* Eos mediates Foxp3-dependent gene silencing in CD4+ regulatory T cells. *Science (New York, N.Y.)* **325**, 1142–6 (2009).

38. Crawford, A. *et al.* Molecular and Transcriptional Basis of CD4+ T Cell Dysfunction during Chronic Infection. *Immunity* **40**, 289–302 (2014).

Methods

Cell lines and Cell line Culture. 293T (cat.#CRL-3216) and Jurkat cells (cat.#TIB-152) were obtained from ATCC. 293GT cells (GripTite 293 MSR cell line cat.#R79507) and HEK293A cells (cat.#R70507) were obtained from ThermoFisher. All cell lines were grown in a humidified incubator held at 37 ^{o}C and 5% CO_2. 293T cell lines were cultured in Dulbecco's Modified Eagle Medium (Invitrogen Cat.#11995-040) supplemented with 10% fetal bovine serum (FBS) and 1% penicillin-streptomycin (Invitrogen cat.#15140-122) and Jurkat cells were cultured in RPMI 1640 medium (ThermoFisher cat.#11875-093) supplemented

with 10% fetal bovine serum and 1% penicillin-streptomycin. All cell lines tested negative for mycoplasma contamination.

Making 293GT CRBN knockout cell line. 293GT CRBN knockout cells were made using CRISPR-Cas9 as follows: A guide RNA targeting CRBN (CCTGTATGCAAGAACAGCAA) was cloned into a vector (pU6-aar1gRNA-nlsSpycas9nls-2apuro) that uses the U6 promoter to express the gDNA, and a CMV promoter to express both *S.pyogenes* Cas9 enzyme (codon optimized for expression in human cells) and a puromycin-resistant selectable marker. 293GT cells were transfected with the CRBN gDNA/CAS9 expressing plasmid and grown for three days in the presence of puromycin (2 µg/ml). Cells were replated in non-selective medium and single colonies were isolated for genomic DNA preparation and sequencing verification. A CRBN knock out clone where all copies of CRBN contain frameshifting insertion mutations was used for all future experiments.

Prolabel protein degradation assays. Cell lines stably expressing ProLabel gene of interest fusions were constructed as follows: A pLenti ProLabel gateway vector was made by inserting DNA sequence encoding the DiscoverX ProLabel tag[39,40] (MSSNSLAVVLQRRDWENPGVTQLNRLAAHPPFASWRNSEEARTDRPSQQLRSLNGE) downstream of the CMV promoter in the pLenti6.2/V5-DEST™ Gateway™ Vector (ThermoFisher Scientific, cat.# V36820). The IKZF1, IKZF2, IKZF3, IKZF4, IKZF2(H141Q), RIPK2, SALL4 and GSPT1 genes were cloned from Gateway entry vectors into the pLenti ProLabel vector using Gateway LR clonase (ThermoFisher cat.#11791019) and all DNA inserts were sequence verified. Viral particles were made by transfecting 293T cells with pLenti Prolabel vectors and plasmids from the Invitrogen™ ViraPower™ Lentiviral Packaging Mix (Invitrogen™ cat.#K497500). 293GT or 293GT CRBN KO cell lines were infected with viral particles carrying the ProLabel tagged genes of interest and selected with 5 µg/mL Blasticidin S HCl (ThermoFisher cat.#A1113903) for 2 weeks to make stable cell lines.

Prolabel degradation assay: ProLabel fusion expressing cell lines were trypsinized, diluted in growth medium to a concentration of 1.0 x 10^6 cells/ml, plated in solid white 384 well plates (17.5 µL per well) (Corning, cat.#3570) and incubated for 24 hours. Test compounds were serially diluted in DMSO and further diluted 25X into growth medium. Cells were treated with 2.5 µL of diluted test compounds and incubated for another 24 hours (final DMSO concentration 0.5%). Plates were removed from the incubator and equilibrated at room temperature for 30 minutes. ProLabel substrate was added according to the manufacturer's instructions (DiscoverX PathHunter Prolabel Detection Kit, User manual: 93-0180) and the plates were incubated for three hours at room temperature. Luminescence was measured using an Envision Multilabel reader (150 ms). Readings from all DMSO wells were averaged and each compound treated well was normalized to DMSO. Results were plotted in GraphPad PRISM 9 and data were fit using the non-linear fit module (4-parameter- log dose versus response) to determine IC_{50} values.

Nanobit recruitment assay. CRBN was cloned into Promega SmBiT Flexi vector pFN35K and IKZF1 and IKZF2 were cloned into Promega LgBiT Flexi vector pFN33K following the Promega protocol (N2015, NanoBiT Protein:Protein Interaction System Technical Manual)[41]. All DNA inserts were sequence verified. 293T cells were transfected as follows: 20 µg of a mixture containing a 1 to 3 ratio of smBiT CRBN and lgBiT IKZF plasmid was added to 1 mL of OptiMEM medium (ThermoFisher cat.#31985062), mixed with 60 µL FuGene HD transfection reagent (Promega, cat.#E2311) and incubated at room temperature for 20 minutes. 293T cells were trypsinized and diluted in growth medium to a concentration of 1.0 x 10^6 cells/mL and the transfection reagents were added to 10 mL of cells. After mixing, cells (18.5 µL per well) were plated into 384 well solid white plates (Corning, cat.# 3570) and incubated for 24 hours. A 20 mM stock (in DMSO) of NAE1 inhibitor MLN4924 (AdipoGen, cat.#905579-51-3) was diluted into growth medium to a concentration of 10 µM and 2.5 µL was added to each well to a final concentration of 1.19 µM and incubated for 24 hours. Test compounds were serially diluted in DMSO and further diluted 25X into growth medium. Cells were treated with 3.0 µL of diluted test compounds and incubated for 10 minutes at room temperature (final DMSO concentration 0.5 %). 6 µL of NanoBiT substrate (Promega, Nano-Glo® Live Cell Reagent, cat.#N2011) was added to each well and the plates were incubated for 30 more minutes at room temperature. Luminescence was measured using an Envision Multilabel reader (150 ms). Readings from all DMSO wells were averaged (DMSO = 100%) and each compound treated well was normalized to DMSO. Results were plotted in GraphPad PRISM 9 and data were fit using the non-linear fit module (4-parameter- log agonist versus response). The Amax values were noted as a measure of the amplitude of the recruitment and the compound concentration at y= 400% (four times the DMSO control) was noted as a relative measure of potency.

Jurkat cell and T-cell endogenous IKZF2 degradation assay. Jurkat cells or primary CD25-enriched T cells were plated at a density of $5x10^4$ cells per well in 96-well round bottom plates. Compounds were obtained from 10 mM stock solution in DMSO with final concentrations decreasing from 10 µM down 3-fold over 8 points, in duplicates. DMSO alone was used as a control in a similar dilution series. For assays on CD25+ primary T cells, 50 IU/mL rhIL-2 was added to the culture.

After 18-24 hours of culture, the cells were collected and stained with LIVE/DEAD® fixable viability dye (Life Technologies, cat. #L34974), washed and fixed with FOXP3 fix/perm buffer (Life Technologies, cat. #00-5523-00) followed by intracellular staining with anti-IKZF2-PECy7 (clone 22F6, BioLegend) and anti-Ikaros-BV421 (clone 16B5C71, BioLegend), and for primary cells with anti-FOXP3-APC (clone 236A/E7, eBioscience). Samples were acquired on a BD LSRFortessa flow cytometer (BD Biosciences). Analysis was performed using the by FlowJo™ Software (BD Life Sciences), and results were graphed using Prism 8 software (GraphPad Prism). IKZF2 median fluorescence intensity (MFI) and IKZF1 MFI were measured in cell lines, and %IKZF2+ FOXP3+ cells was measured in primary T cell cultures and normalized to the average of DMSO-treated samples for that culture.

Expression proteomics. *Sample preparation: Cell culture, lysis, digestion, Tandem Mass Tag (TMT) labeling:* Three million Jurkat cells were plated in 100 mm tissue culture dishes containing 10 mL of growth medium. Cells were exposed to DKY709 (2.5 µM final concentration) or DMSO by adding 10 µL of a 2.5 mM DKY709 stock solution (in DMSO) or 10 µL of pure DMSO as a control. After 16 hours of incubation, cells were collected into sterile 15 mL conical tubes, pelleted by centrifugation (1000 rpm for 5 minutes) and the medium was removed by aspiration. Jurkat cells were resuspended in 10 mL of ice-cold PBS (Phosphate Buffered Saline), pelleted by centrifugation (1000 rpm for 5 minutes at 4 ^{o}C) and the PBS was removed by aspiration. The pellet was resuspended in 0.5 mL of ice-cold PBS and transferred to an eppendorf tube. Cells were pelleted in a microfuge at 1000 RPM for five minutes at 4 ^{o}C. The PBS was aspirated, and the washed pellets were frozen at -80 ^{o}C for proteomic analysis.

Cell pellets were lysed in 100 µL iST-NHS lysis buffer and sonicated to shear and break the DNA aggregates. After centrifugation, the protein concentration was measured by following a BCA™ Protein Assay Kit (Thermo cat.#23227). All lysate protein concentrations for each condition were normalized to one concentration of 100 µg. An automated sample prep system called the PreON, developed by PreOmics, Inc. was then used to process the lysed material from digestion to TMT labelling and purification of peptides, in a fast and streamlined workflow[42,43]. The PreOn automated platform enables reproducible, high throughput sample preparation, of up to 16 samples, using reagents provided in the iST-NHS kit (PreOmics GmbH cat.#00030). Digestion of 100 µg protein was performed for a total incubation time of 2 hours at 37 ^{o}C. Each sample was then labelled with a tandem mass tag (TMTpro^{TM}, Thermo cat.#A44522) at a ratio of 5 µg tag to 1 µg protein for a total of 90 minutes at room temperature. The reaction is then quenched with 0.5% hydroxylamine TMT-labelled samples and are then combined and distributed evenly in cartridges to purify peptides. Final eluates were placed in a speed-vacuum to dry overnight.

LC-Fractionation: Following elution and concentration of peptides in a Genevac EZ 2.3 Elite vacuum concentrator, 530 µg of pooled multiplexed sample was fractionated by an offline high-pH fractionation system (Agilent HPLC 1200 series; Waters XBridge C18 3.5 µm, 150 mm x 2.1 mm column). The peptide separation was achieved with a ramp of 5-45% mobile phase B (90% acetonitrile, 5 mM ammonium formate buffer prepared from ammonium hydroxide, pH 10) in 74 min, with increase to 60% B for a total of 77 min effective gradient. Each sample was fractionated into ninety-six fractions and then manually pooled into twenty-four final fractions. Individual fractions were subsequently concentrated, and peptides reconstituted in 0.1% formic acid to 1 µg/µL.

Online LC-MS Chromatography: Tryptic peptides in each fraction were analysed using an Orbitrap Fusion™ Lumos Eclipse™ Mass Spectrometer (Thermo) equipped with an IonOptix Aurora 25 Column (1.6 µm C18, 75 µm ID x 25 cm) at an isocratic flow of 400 nL/min with a 83 min gradient of 6-35% mobile phase B (80% acetonitrile with 0.1% formic acid) using the synchronized precursor selection (SPS) mass spectrometry to the third (MS3) mode coupled with Real Time Search (RTS) function. Briefly, the first

stage of mass spectrometry (MS1) was performed in the Orbitrap and scanned from 400 to 1600 mass to charge (m/z) with a resolution of 120,000. Only ions with charge state from 2+ to 6+ were selected for MS2 scans. The second stage of mass spectrometry (MS2) scan in the iontrap was set to a precursor isolation window of 0.7 m/z and normalized collision energy fixed at 32%. SPS-MS3 scans in the Orbitrap were set to 50,000 with 10 SPS precursors, an isolation window of 2, and a collision energy set to 40%.

LC-MS Data Analysis: Thermo Proteome Discoverer version 2.4 was used to process the raw mass spectrometry files. Briefly, spectra were matched against human fasta file downloaded from Uniprot (version July 2019 one gene/one protein with roughly 20,000 human reference proteins appended with common mass spec contaminants such as trypsin) using SequestHT algorithm. Peptide matches with <1% FDR as determined by Percolator were kept generating a list of identified proteins. Next, accepted peptides with TMT scores as follows SPS mass matched 65%, precursor contamination 50%, minimum average reporter ion with signal/noise greater than 10 were used for protein quantitation utilizing only non-shared peptides. In-house collection of python and R scripts were used for further data normalization, e.g. adjustment for difference in total protein loaded per TMT channel, and also for assessing protein response upon compound treatment and fold change compared to DMSO treatment (n = 3 biological replicates per treatment) using R Limma package[44]. Resulting p-values were corrected using commonly used Benjamini-Hochberg procedure. For clarity, the volcano plots are visualized as unadjusted p-values.

CRBN binding Assay. CRBN binding by compounds was determined by their ability to compete binding of a BodipyFL conjugated lenalidomide fluorescent probe[45] as measured by fluorescence polarization. Test compounds were diluted in 90 % (v/v) DMSO/water and 100 nL was transferred to 384 well plates (Black Microtiter 384 Plate, round well; cat.#95040020 Thermo Electron Oy, Finland). 5 µL of CRBN/DDB1 protein solution (100 nM final concentration) in assay buffer (50 mM Tris/HCl at pH 7.4, 100 mM NaCl, 0.1 % (w/v) Pluronic F-127 and 1 mM TCEP) was added to each well and incubated at room temperature for 45 minutes. The binding measurement was started by addition of 5 µL of fluorescent probe in assay buffer (5 nM final concentration) and the final DMSO concentration was 0.9% (v/v). After 45 minutes at room temperature, fluorescence polarization was measured using a PHERAstar reader (BMG Labtech, Offenburg, Germany) with excitation at 485 nm and emission at 520 nm. EC_{50} values were calculated from the plot of percentage of protein saturation versus the test compound concentration by a logistics fit according to y = A2+(A1– A2)/(1+(x/ EC_{50})^ p), where y is the %-saturation value at the test compound concentration, x. A1 is the lowest saturation value, i.e. 0 %, and A2 the maximum saturation value, i.e. 100 %. The exponent, p, is the Hill coefficient.

CRBN cellular engagement assay. The ability of compounds to bind CRBN in cells was determined by measuring a compound's ability to block the effect of a CRBN binding bifunctional degrader. 293GT ProLabel-RIPK2 cells were trypsinized, diluted to 1.0 x 10^6 cell/mL in growth medium, plated in solid

white 384 well plates (17.5 µL per well) (Corning, cat.#3570) and incubated overnight. Test compounds were serially diluted in DMSO, further diluted 24X into growth medium and 2.5 µL of diluted test compounds were added to each well. Shortly afterwards, 2 µL of a lenalidomide-RIPK2 bifunctional degrader (**probe 1**) (Supplementary, Compounds synthesis and characterization, Scheme 6) was added to each well (final concentration 50 nM probe 1, 0.55% DMSO) and the plates were incubated for 24 hours at 37 degrees. Plates were removed from the incubator and equilibrated at room temperature for one hour. ProLabel substrate was added according to the manufacturer's instructions (DiscoverX PathHunter Prolabel Detection Kit, User manual: 93-0180) and the plates were incubated for three hours at room temperature. Luminescence was measured using an Envision Multilabel reader (200 ms). Readings from all DMSO/probe 1 treated wells were averaged and were the negative control value (NC) and readings from 10 µM pomalidomide/ probe 1 treated wells were averaged and were the active control value (AC). Percent activity was calculated by the following equation 100[(x-NC)/(AC-NC)]. Results were plotted and IC_{50} values were calculated using the Novartis Helios software package.

HiBit protein degradation assays

Cell lines stably expressing HiBit-gene of interest fusions[46] were constructed as follows: The lentiviral vector pLenti6.2/V5-DEST Gateway Vector (ThermoFisher cat.#V36820) was modified to express either mCherry-CHYSEL-HiBiT at the N-terminus of the protein of interest, or HiBiT-CHYSEL-mCherry at the C-terminus of the protein of interest. IKZF1 and SALL4 open reading frames were cloned to generate N-terminal HiBiT fusions, while GSPT1 was cloned to generate C-terminal HiBiT fusions. Cloning was performed using Gateway LR clonase (ThermoFisher cat.#11791019), and all DNA inserts were sequence verified. Virus was made as described above and used to infect 293GT cells (ThermoFisher Scientific cat.#R79507) and HiBit fusion stable cell lines were generated and maintained in the presence of 10 µg/ml of Blasticidine S HCl (ThermoFisher cat.#A1113903).

HiBit stable cell lines were trypsinized and diluted in growth medium to a concentration of 5 x 10^4 cells/mL for GSPT1-HiBit, 4 x 10^5 cells/mL for HiBit-IKZF1 and 2 x 10^5 cells/mL for HiBit-SALL4 expressing cells. 5 µL of cells were plated into wells of solid white 1536 well plates (Greiner cat.# 789173-A) and incubated overnight. Test compounds were serially diluted in DMSO and 10 nL of compound was dispensed directly into the wells using an Echo dispenser. After 20 hours of incubation, plates were removed from the incubator and allowed to equilibrate at room temperature for 30 minutes. 3 µL of Nano-Glo® HiBit Lytic Reagent (Promega cat.#N3050) was added to each well using a single tip bottle valve and plates were incubated for 20 minutes at room temperature. Luminescence was measured using a PHERAstar reader and readings from all DMSO wells were averaged and each compound treated well was normalized to DMSO. Results were plotted and IC_{50} values were calculated using the Novartis Helios software package.

High throughput solubility measurements. The high-throughput (HT) equilibrium solubility assay was performed after Zhou et *al.*[47]. Briefly, aliquots of 10 mM DMSO stock solution were plated and DMSO was removed under temperature and vacuum. pH 6.8 potassium phosphate buffer (67 mM) was added to the 96-well plate for a compound target concentration of 1 mM. The plate was sealed, incubated on a shaker at 1350 RPM and ambient temperature for 16-24 hours, and then centrifuged for 20 min at 3750 RPM to pellet the precipitate. The supernatant was transferred to another plate and centrifuged a second time. Supernatant was diluted 200-fold with 50:50 acetonitrile/water and a 4-point calibration curve was constructed using 50:50 acetonitrile/water. Analysis of the supernatant concentration was performed based on the calibration curve, using an Agilent RapidFire-MS/MS mass spectrometer system.

MDCK-LE permeability assay. Compound permeability was measured following the method described by Huth and co-workers[48].

Protein production and purification. Full-length human CRBN constructs (residues 1-442) tagged with N-terminal ZZ-His was co-expressed with full-length human DDB1 (residues 1-1140) in Sf21 cells (Expression Systems) with 100 μM zinc acetate supplemented medium. Frozen cells were lysed by homogenization at pH 7.5. The soluble fraction was purified with histidine-affinity, ion-exchange and size-exclusion chromatography. Protein was concentrated to ~30 mg/mL in 20 mM HEPES, pH 7.0, 250mM NaCl, 2mM TCEP. For SPR binding assay, full-length human CRBN constructs (residues 1-442) as generated with a non-cleavable N-terminal Avi-tag with a 6xGS linker in addition to the upstream solubility tag. Avi-tagged CRBN was labeled with 100% efficiency with biotin using BirA enzyme[49].

Human IKZF2 constructs (137-162 and 137-192) tagged with Twin-Strep-ZZ in a pET vector. IKZF2 constructs were expressed in *E. coli* BL21 (DE3) Star cells (Life Technologies cat.# C601003) in TB medium supplemented with 100 μM zinc acetate. Frozen cells were lysed by sonication at pH 8.0. The soluble fraction purified with Strepavidin-affinity, ion-exchange and size-exclusion chromatography. Protein was concentrated to 3-4 mg/mL in 20 mM HEPES, pH 6.8, 100mM NaCl.

SPR binding measurements. The binding of DKY709 and IKZF2 zinc finger proteins to CRBN or CRBN:DKY709 complexes, respectively, was measured on a Biacore 8k instrument in PBS buffer at pH 7.2 containing 5% glycerol, 150 mM NaCl, 0.01% P20 detergent, and 1 mM TCEP. For the binding of DKY709 to DDB1:N-avi-CRBN, this buffer contained 2% DMSO, and 1 mM EDTA. For the binding of IKZF2 proteins to DDB1:N-avi-CRBN:DKY709 complex, the Biacore ABA method was used to measure binding data for solutions with 5 mM DKY709 throughout the acquisition of baseline, IKZF2 association, and IKZF2 dissociation, where only the solutions for the association phase contain a 2X dilution series of IKZF2 proteins. Data analysis was performed with Biacore Insights software to normalize data relative to the

baseline injections. The temperature was 15 degrees Celsius, and the flow rate was 30 µL/minute. DDB1:N-avi-CRBN, where the avi-tag is labeled with biotin, was loaded onto a streptavidin-coated Biacore sensor to ~6000-7000 RU, and the surface was exposed to 1 mM biocytin to block unoccupied streptavidin sites prior to analyses.

CRBNΔ40/DDB1ΔBPB:DKY709:IKZF2(ZF2) ternary complex crystallography.

DKY709 was first added (2 mM) to CRBNΔ40/DDB1ΔBPB in 20 mM HEPES pH7.0, 250 mM NaCl, 2 mM TCEP. After incubation on ice for 30 minutes, 3X IKZF2(ZF2) (137-162) (formulated in 25 mM MES pH6.5, 100 mM NaCl, 10 mM $ZnCl_2$) was added and further incubated on ice for 30 minutes prior to crystallization screen. A single crystallization condition of CRBNΔ40/DDB1ΔBPB:DKY709:IKZF2(ZF2) was identified from the Qiagen Protein Complex Suite G10 (1.6 M Potassium/Sodium phosphate pH 6.5) at 4 °C using the hanging drop vapor diffusion method, after 1 week of incubation. Harvested crystals were flash cooled in liquid nitrogen following gradual equilibration into cryo protectant solution consisting of 25% (v/v) ethylene glycol supplemented to mother liquor. Diffraction data were collected at Advanced Light Source beamline 5.0.2 (λ = 1.0000 Å) using a Pilatus 6M detector and processed using process (Global Phasing Ltd.). The crystals belonged to space group P 61 2 2 with unit cell parameters a = 180.9, b = 180.9, c = 555.9 Å and α = 90°, β = 90°, γ = 120° and contained two copies of the ternary complex per asymmetric unit. The structure was solved by molecular replacement using PHASER[50] with coordinates derived from the CRBNΔ40/DDB1ΔBPB:Pomalidomide:IKZF1(ZF2) complex (PDB entry 6H0F)[25] as search models. Subsequent iterative model building and refinement was performed using COOT[51] autoBUSTER (Global Phasing Ltd.) and PHENIX[52]. The structure was refined to Rwork and Rfree values of 20.8% and 24.0%, respectively, with 99.5% of the residues in Ramachandran favored and allowed regions as validated with MOLPROBITY[53].

Treg procurement, isolation and expansion. Blood products obtained from healthy donors was purchased from Bioreclamation IVT (NJ), Hemacare (CA) or Stemcell Technologies (MA) in accordance with their respective IRBs. Informed consent was obtained from all participants and all ethical regulations were respected. Peripheral Blood mononuclear cells (PBMC) of were isolated from blood using density centrifugation on Ficoll-Paque (Millipore Sigma cat.#GE17-1440-03) following manufacturer instructions. CD4 enrichment by negative selection followed by CD25 enrichment by positive selection were performed using the human CD4 T cell isolation kit (cat.#130-096-533) and human CD25 microbeads (cat.#130-092-983) from Miltenyi Biotec (Cambridge, MA) according to manufacturer's instructions. Isolated Tregs were expanded for 8-14 days in the presence of DKY709 or DMSO, using Treg expander beads (ThermoFisher, cat.#11129D) or T-cell activator beads (ThermoFisher, cat.#11161D) at a 4:1 or 3:1 ratio, respectively, in the presence of 500 U/mL rhIL-2.

Treg suppression assay. Expanded Treg cells were dispensed in co-culture with CFSE-labelled PBMCs at various Treg:PBMC ratios in the presence of T-cell activator beads or soluble anti-CD3 antibody (30 ng/mL, OKT3, Thermofisher cat.# 16-0037-81). After 3-4 days of incubation, proliferation was assessed by analysing CFSE dye dilution using flow cytometry. Analysis was performed using a BD Fortessa (BD Biosciences; BD LSRFortessa), the by FlowJo™ Software (BD Life Sciences), and results were graphed using GraphPad Prism. Teff cells that had proliferated during the co-culture were identified as having diluted CFSE and data were plotted as the proportion of $CFSE^{low}$, proliferated cells in the final culture. CFSE-labelling of PBMC was performed according to manufacturer instructions (Invitrogen cat.#C34554).

Teff cell exhaustion assay. T cell functional exhaustion was modelled in vitro using a repeated stimulation protocol as previously described[54]. T cells were enriched from PBMCs using the Pan T cell isolation kit and an LS separation column from Miltenyi Biotec according to manufacturer's instructions. Cells were plated in the presence of DKY709 at indicated concentrations, or DMSO, and stimulated with CD3/CD28 stimulation beads at 3:1 ratio (Thermofisher, cat.#11161D). On day 5 of culture, cells were collected, and beads removed, followed by re-plating with fresh beads in the presence of compound at the same concentration. After 5 days or restimulation, cells were treated with Cell stimulation cocktail (Life Technologies, cat.#00-4975-93) for 4 hours, then collected and stained for viability (live/dead fixable dye, Life Technologies, cat.#65-0865-14) and cell surface markers Cd3-FITC (OKZT3), CD4-BUVXX (SK3), CD8-BV510 (SK1) and PD1-BV786 (EH12.2H7), followed by fixation using the Foxp3 staining buffer kit from Ebioscience and intracellular staining for Helios-PE-Dazzle594 (22F6), IL2-BV650 (MQ1-17H12) and IFNg-AlexaFluor700 (4S.B3). Cells were acquired on a BD LSRFortessa flow cytometer (BD Biosciences). Analysis was performed by FlowJo™ Software (BD Life Sciences), and results were graphed in GraphPad Prism 8.

IL-2 production in Jurkat cells. Jurkat cells were plated at $5x10^4$ cells/mL in 96-well round bottom plates. Compound was added at decreasing dilution from 10 µM down 5-fold, 8-points, in duplicates. After 24 hours, supernatants were collected and concentration of IL-2 was measured using MSD Human IL-2 Tissue Culture Kit (cat.#K151AHB-4, Mesoscale). Data was normalized to the DMSO-treated wells.

***In vivo* mouse humanization and tumor xenograft.** Immunodeficient female mice of the NOD-SCID-IL2Rγ-/- (NSG) strain obtained from Jackson Laboratories and the study was carried out in accordance with the guidance from Novartis IACUC board of regulations, respecting all ethical regulations. Mice were subjected to 250 cGy of whole-body irradiation or administered bisulfan at a dose of 30 mg/kg IP and subsequently each engrafted with 50,000 hematopoietic stem cells (HSCs), from one of five donors,

derived from human umbilical cord blood. Engraftment ranged from 19.3% to 98.1% hCD45+ cells at study enrolment. MDA-MB231 cell suspension in matrigel (200 µL or 10 x 106 cells per mouse) was implanted subcutaneously in NSG mice and tumor volume was monitored twice weekly. Seven days post MDA-MB231 implantation, daily oral dosing of DKY709 (100 mg/kg) and weekly intraperitoneal injection of PD-1 blocking antibody (PDR001) were initiated. After 21 days on study, blood and tumor samples were collected for terminal phenotype analysis. Blood samples were treated with ACK Lysing Buffer (Gibco, cat.#A1049201) for red blood cell lysis. Tumors were mechanically dissociated and digested using Liberase TM (Sigma-Aldrich, cat.#LIBTM-RO) / DNAse I (Roche, cat.#10104159001) with additional mechanical dissociation using the gentleMACS Dissociator (Miltenyi Biotec). Cell suspensions were then surface stained for viability (live/dead ebioscience, cat.#65-0865-14) and using antibodies against CD45-FITC (Hi30), CD8-BV510 (SK1), and CD25-BV421 (BC96) from Biolegend, and CD4-BUV737 (SK3) from BDBiosciences. Cells were fixed using the FOXP3 fix/perm kit (eBioscience, cat.#00-5523-00) and stained intracellularly with antibodies against Helios-Pe-Cy7 (22F6) and FOXP3-APC (236A/E7) from Biolegend and Invitrogen, respectively. Data was acquired using a BD LSRFortessa Cell Analyzer (BD Biosciences), analysed using the by FlowJo™ Software (BD Life Sciences) and plotted in GraphPad Prism.

In vivo **monkey immunization and immunophenotyping.** A non-GLP immunization study with DKY709 dosing was conducted in male cynomolgus monkeys at Covance/LabCorp. The study protocol was approved by the local IACUC board and the study was conducted in compliance with the Animal Welfare Act, the Guide for the Care and Use of Laboratory Animals, and the Office of Laboratory Animal Welfare. The study was carried out respecting all ethical regulations. Male cynomolgus monkeys (2-3 per group, aged 3-5 years) were administered 0.1 mg/kg/day DKY709; 2.5 mg mL KLH and 0.5 mL squalene adjuvant; 2.5 mg KLH, 0.5 mL squalene adjuvant and 0.1 mg/kg/day DKY709; or 2.5 mg KLH, 0.5 mL squalene adjuvant and 3 mg/kg/day DKY709. Animals were first immunized intramuscularly with KLH/Squalene or a vehicle control. On day 5 post immunization, daily oral treatment was initiated with DKY709 or a vehicle control for the indicated groups at the indicated dose, for the remainder of the study (36 days after immunization). Immunized groups received a recall immunization on day 15 after the initial immunization. Blood was collected by venipuncture in K2 EDTA tubes at the indicated timepoints. For assessment of IKZF2 degradation, samples were immediately fixed in 5:1 volume of FOXP3 fixation buffer (cat.#00-5523-00) for overnight fixation. Samples were then washed in BD FACS staining buffer (cat.#554656) and shipped to the analysis facility. Samples were subsequently stained intracellularly for CD3 (SP34-2), CD20 (2H7), CD8 (SK1) (BD bioscience), FOXP3 (236a/e7, ThermoFisher), Helios (22F6), CD16 (3G8) and Ikaros (16B5C71) (BioLegend) prior to acquisition on a flow cytometer (BD Biosciences; BD LSRFortessa). Analysis was performed by by FlowJo™ Software (BD Life Sciences), and results were graphed using GraphPad Prism 8. For assessment of T cell proliferation, blood was collected and immediately processed for surface and intracellular staining as described above with the addition of CD45, CD95, CD28 and KI67-detecting antibodies. Samples were acquired on a BD CANTO II flow cytometer. Analysis of the raw data files was performed using flow cytometry data analysis software Kaluza version 1.5 (Beckman Coulter), and results were graphed using GraphPad Prism 8.

Human clinical trial samples (PK, PD). DKY709 concentration in human plasma collected from the ongoing clinical trial (ClinicalTrials.gov NCT03891953) was measured by a Novartis-proprietary validated LC/MS/MS method to support pharmacokinetic assessment. Blood was drawn into heparin tubes, processed to PBMC and cryopreserved at Covance within 48 hours of collection. PBMC were collected from patients on the trial at C1D1, C1D2, C1D15, and C2D15 predose, and C1D1, C1D15, and C2D15 4 hours postdose. Blood samples were collected from patients by venipuncture at indicated time points and processed for PBMC cryopreservation. For characterization of Helios expression in different immune cell subsets, including T regulatory cells (Tregs), Helios expression was measured by a Novartis-proprietary validated 13-parameter flow cytometry assay. Flow cytometry was performed on cryopreserved PBMC at Navigate BioPharma Laboratory, Carlsbad, CA. PBMCs were thawed, washed with phosphate-buffered saline containing 0.1% sodium azide and 2% fetal bovine serum, and incubated with Fc Receptor Binding Inhibitor (ThermoFisher Scientific). Cells were stained with fixable viability dye (Thermo Fisher Scientific, San Diego, CA), followed by staining with fluorochrome conjugated antibodies. Cells were washed, then prepared for intracellular staining with the Foxp3 / Transcription Factor Staining Buffer Set (ThermoFisher Scientific, Carlsbad, CA), according to the manufacturer's instructions. Intracellular staining was performed, cells were washed with 1x Permeabilization Buffer, then fixed with 0.5% formalin. Stained Samples were acquired on a BD LSRFortessa X-20 (BD Biosciences, San Jose, CA) and data were analysed using FlowJo™ Software (BD Life Sciences). Informed consent was obtained from all participants and all ethical regulations were respected.

Chemical synthesis and characterization. All chemical synthesis procedures and characterization data are provided in the Supplementary Information in the *Compounds Synthesis and Characterization* section.

Statistical Analysis

All statistical analyses were performed using GraphPad Prism unless otherwise stated in the Methods section.

Data availability: The authors declare that the data supporting the findings of this study are available within the publication and its Supplementary Information files or have been deposited in the RCSB Protein Data Bank (PDB, http://www.rcsb.org). Further information available upon request. The PDB accession code for the human DDB1:CRBN:DKY709:IKZF2(ZF2) X-ray co-structure is 7U8F.

Methods-only References:

39. Zhao, X. *et al.* Homogeneous assays for cellular protein degradation using beta-galactosidase complementation: NF-kappaB/IkappaB pathway signaling. *Assay and drug development technologies* **1**, 823–33 (2003).

40. Olson, K. R. & Eglen, R. M. Beta galactosidase complementation: a cell-based luminescent assay platform for drug discovery. *Assay and drug development technologies* **5**, 137–44 (2007).

41. Dixon, A. S. *et al.* NanoLuc Complementation Reporter Optimized for Accurate Measurement of Protein Interactions in Cells. *ACS chemical biology* **11**, 400–8 (2016).

42. van Bergen, W., Heck, A. J. R. & Baggelaar, M. P. Recent advancements in mass spectrometry-based tools to investigate newly synthesized proteins. *Current opinion in chemical biology* **66**, 102074 (2022).

43. Zaro, B. W. *et al.* Proteomic analysis of young and old mouse hematopoietic stem cells and their progenitors reveals post-transcriptional regulation in stem cells. *eLife* **9**, (2020).

44. Ritchie, M. E. *et al.* limma powers differential expression analyses for RNA-sequencing and microarray studies. *Nucleic acids research* **43**, e47 (2015).

45. Arista, L. *et al.* Bifunctional degraders and their methods of use. WO 2021/053495 Al, 1–513 (2021).

46. Schwinn, M. K. *et al.* CRISPR-Mediated Tagging of Endogenous Proteins with a Luminescent Peptide. *ACS chemical biology* **13**, 467–474 (2018).

47. Zhou, L., Yang, L., Tilton, S. & Wang, J. Development of a high throughput equilibrium solubility assay using miniaturized shake-flask method in early drug discovery. *Journal of Pharmaceutical Sciences* **96**, 3052–3071 (2007).

48. Huth, F. *et al.* Predicting Oral Absorption for Compounds Outside the Rule of Five Property Space. *Journal of pharmaceutical sciences* **110**, 2562–2569 (2021).

49. Fairhead, M. & Howarth, M. Site-specific biotinylation of purified proteins using BirA. *Methods in molecular biology (Clifton, N.J.)* **1266**, 171–84 (2015).

50. McCoy, A. J. *et al. Phaser* crystallographic software. *Journal of Applied Crystallography* **40**, 658–674 (2007).

51. Emsley, P., Lohkamp, B., Scott, W. G. & Cowtan, K. Features and development of *Coot*. *Acta Crystallographica Section D Biological Crystallography* **66**, 486–501 (2010).

52. Liebschner, D. *et al.* Macromolecular structure determination using X-rays, neutrons and electrons: recent developments in Phenix. *Acta crystallographica. Section D, Structural biology* **75**, 861–877 (2019).

53. Williams, C. J. *et al.* MolProbity: More and better reference data for improved all-atom structure validation. *Protein Science* **27**, 293–315 (2018).

54. Dunsford, L. S., Thoirs, R. H., Rathbone, E. & Patakas, A. A Human In Vitro T Cell Exhaustion Model for Assessing Immuno-Oncology Therapies. in 89–101 (2020). doi:10.1007/978-1-0716-0171-6_6.

Figures

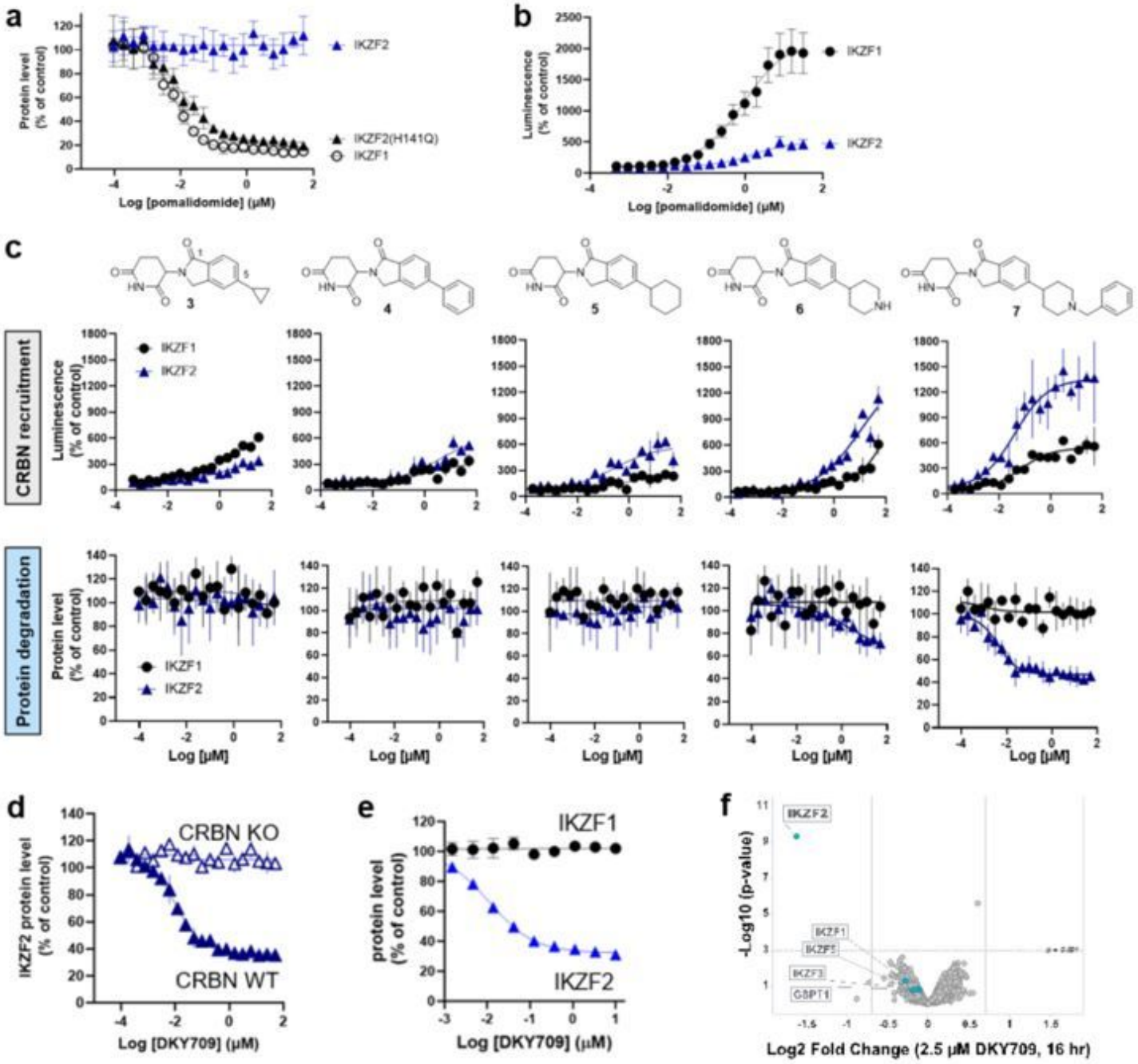

Figure 1

Discovery of DKY709 and characterization of DKY709 selectivity. a, Levels of IKZF1, IKZF2 or IKZF2 H141Q mutant protein in engineered 293T cells following overnight treatment with increasing doses of pomalidomide (**1**). Data are mean ± s.d. (n = 4 per group) from a single experiment. **b**, Cellular recruitment of IKZF1 or IKZF2 to CRBN observed with increasing doses of pomalidomide (**1**). Data are mean ± s.d. (n = 8 per group) from a representative experiment. The experiment was performed independently two times. **c**, Development of DKY709 through structure-activity optimization: IKZF1 and IKZF2 cellular recruitment to CRBN and IKZF1 and IKZF2 cellular protein levels in 293T cells were measured in the presence of increasing doses for each compound in the series. Recruitment data are mean ± s.d. (n = 2 per group) from a representative experiment. Degradation data are mean ± s.d. (n = 4 per group) from a representative experiment. Each experiment was performed independently at least two times. **d**, IKZF2 protein levels in the presence of increasing doses of DKY709 in CRBN wild-type and CRBN knockout (KO) 293T cells. Data are mean ± s.d. (n = 2 per group) from a representative experiment. The experiment was performed independently three times. **e**, IKZF2 and IKZF1 protein levels (mean fluorescence intensity, MFI) measured by FACS in Jurkat cells treated 16-20 hours with increasing doses of DKY709. Data are mean ± s.d. (n = 2 per group) from a representative experiment. The experiment was performed independently 3 times. **f**, Quantitative proteomics profiling of Jurkat cells treated for 16 hours with 2.5 μM of DKY709 or DMSO. Volcano plot shows downregulation of IKZF2 upon DKY709 treatment compared to vehicle (protein FDR < 1%, $n = 3$ biological replicates per treatment). Log_2(fold change) difference between means of treated vs. DMSO plotted against p-values calculated using Limma. Lines in the plot indicate significant cutoffs: p-value < 0.001 and absolute [Log_2(fold change)] > 0.7.

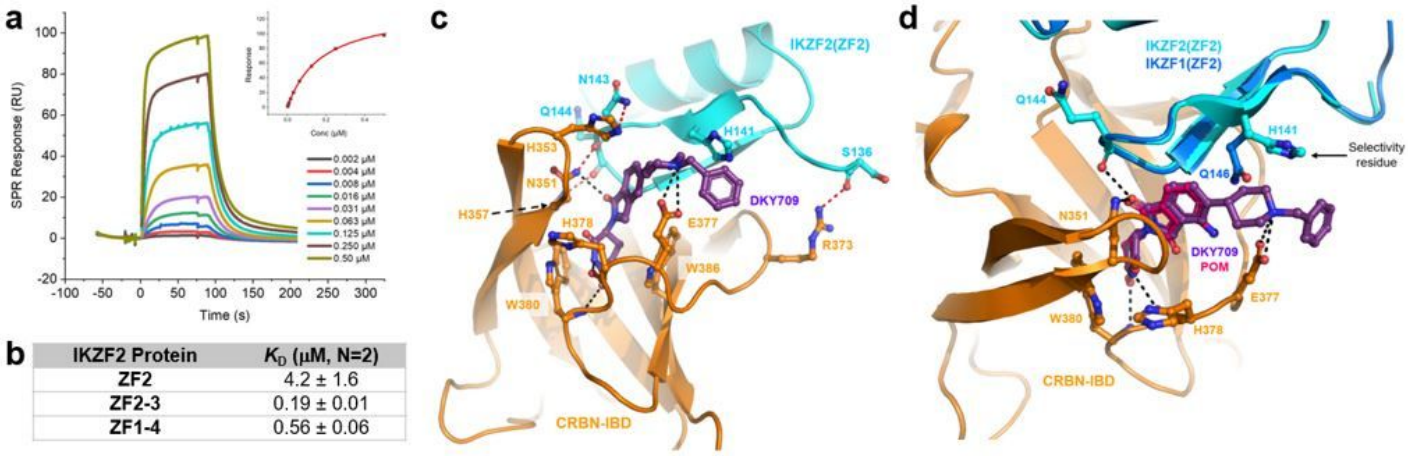

Figure 2

Biophysical and structural characterization of IKZF2 zinc finger recruitment to CRBN by DKY709. a, SPR plot for the binding of IKZF2(ZF2-3) to DDB1:CRBN:DKY709 complex and corresponding response vs

concentration plot for K_D determination from a 2X dilution series from 0.001-0.5 mM IKZF2 in the presence of 5 mM DKY709. **b**, SPR binding affinities of IKZF2 constructs ZF2, ZF2-3, ZF1-4 to the DDB1:CRBN:DKY709 complex. **c**, Ligand binding pocket in DDB1:CRBN:DKY709:IKZF2(ZF2) complex determined at 3.15 Å resolution. Hydrogen bonds and salt bridges are shown as dashed lines to DKY709 (black) and between CBRN and IKZF2(ZF2) (red). **d**, Comparison of DKY709-induced binding of IKZF2(ZF2) (PDB ID 7U8F) to pomalidomide induced binding of IKZF1(ZF2) (PDB ID 6H0F).

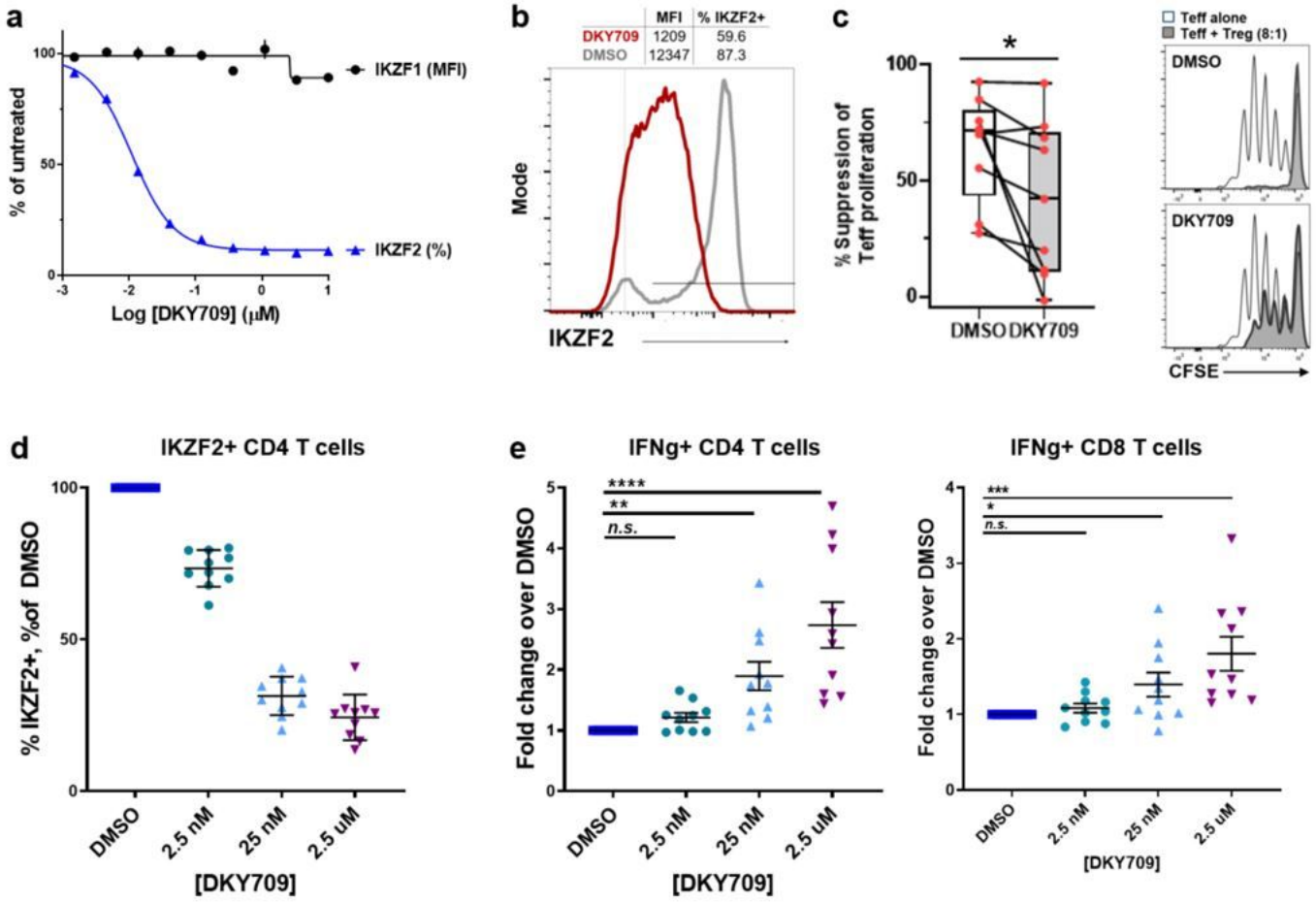

Figure 3

Effects of DKY709 treatment on T cells and Tregs *in vitro.* **a**, Levels of IKZF2 and IKZF1 in primary human Tregs after 24 hours in vitro treatment with DKY709. Data is shown as mean of duplicates +/- SD in a representative experiment of at least 3. **b**, Levels of IKZF2 in primary human Tregs expanded in vitro in the presence of 10 mM DKY709 or DMSO as indicated by Median fluorescence intensity (MFI) (upper left corner) or percent positive fraction. Data is representative of over 10 independent experiments. **c**, Suppression of Teff proliferation by primary human Treg cells expanded in the presence of DKY709 or DMSO. Data is shown as 8 independent experiments/donors (left), with median+/- IQ range at 1:8 Treg:PBMC co-culture ratio. Data is normalized to proliferation of Teff in PBMCs alone for each donor. *

p<0.05. Groups were compared using 2-tailed paired parametric T-test. (right) Representative flow cytometry overlays showing proliferation as denoted by CFSE dilution in Teff cells alone or in co-culture with Tregs expanded with the indicated compound. **d**, IKZF2 expression and **e,** IFNg production in IKZF2+ cells upon DKY709 treatment in indicated subset of dysfunctional Teff cells induced in vitro by repeated TCR stimulation. Data shown is pooled from 9 independent experiments and donors. Representative flow cytometry plots shown in Extended Data Fig. 3c. Mean +/- SEM is shown. Statistical comparison to DMSO treated group performed by Kruskal-Wallis test. * p<0.05, ** p< 0.005, *** p<0.0005, **** p<0.0001.

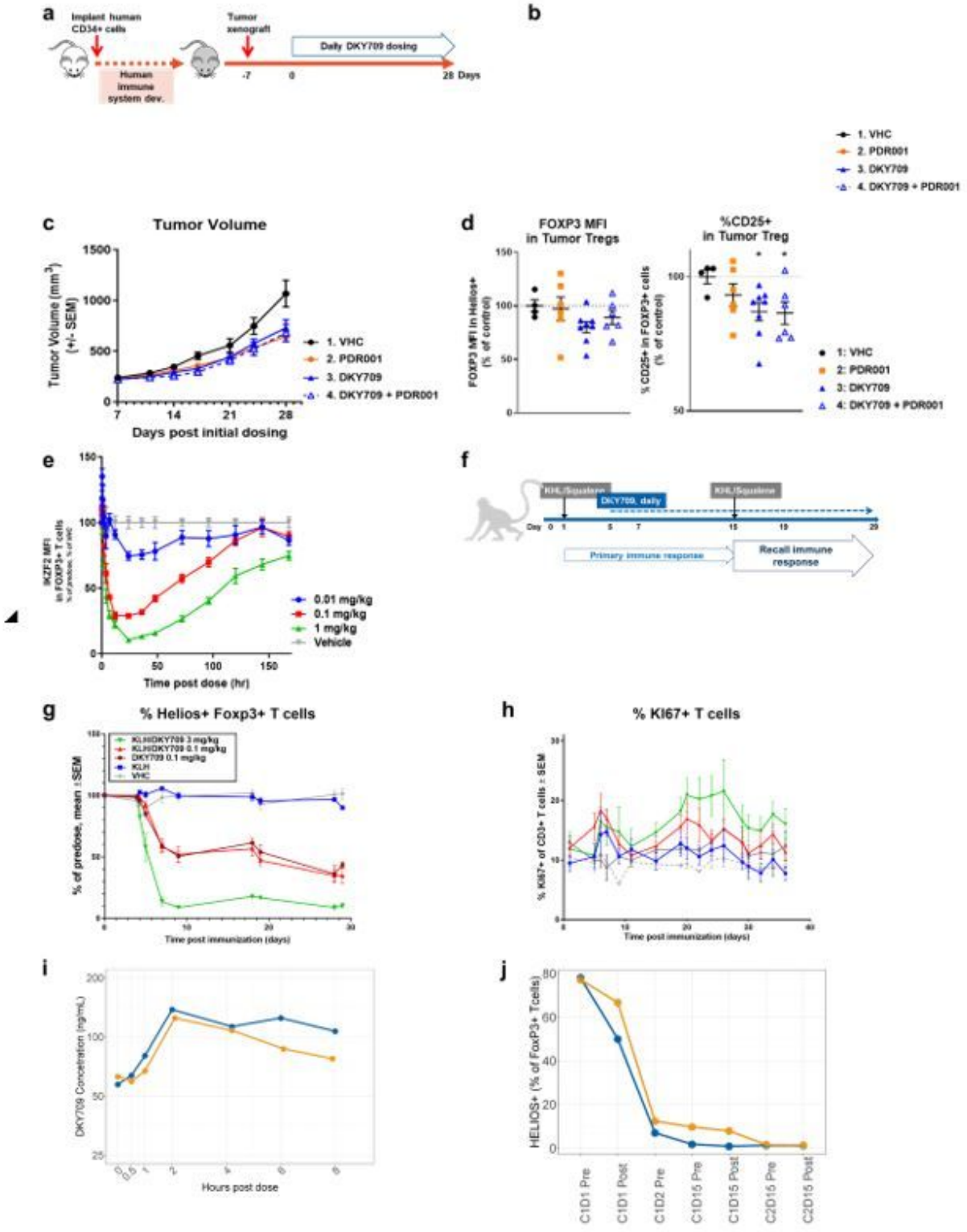

Figure 4

Effect of DKY709 treatment on immune response *in vivo.* **a**, Study schematic. **b**, In vivo degradation of IKZF2 in primary Treg cells in humanized mouse model of MDA-MB231 tumor xenograft in tumor-infiltrating (left) and blood (right) Foxp3+ Treg cells. **c**, Tumor growth reduction induced by daily DKY709 treatment (100 mg/kg) alone or in combination with PD-1 blockade in MDA-MB231 xenograft model. **d**, Reduction of Treg fitness markers FOXP3 MFI and CD25 expression in tumor-infiltrating Tregs upon DKY709 in vivo treatment (same as a, b). Data is shown as mean ± SEM, n=8 mice per group. **e**, IKZF2 level in Tregs as assessed by FACS in blood of cynomolgus monkey after single oral dose (indicated) of DKY709. Data is shown as mean ± SEM for n=3 monkeys per group. **f**, Study schematic. **g**, IKZF2 levels in peripheral Tregs upon daily administration of indicated doses of DKY709 in monkeys immunized with adjuvanted KLH (n = 2-3 monkeys per group). **h**, Proliferation of peripheral T cells as assessed by levels of KI67 expression in CD3+ cells in blood, upon daily administration of indicated doses of DKY709 in monkeys immunized with adjuvanted KLH (n = 2-3 monkeys per group). **i**, Human pharmacokinetics for 2 enrolled patients receiving DKY709 orally at 20 mg daily. Concentration of DKY709 were measured in patient plasma over an 8-hour time period following daily oral administration for approximately 6 weeks. **j**, IKZF2 levels in human Tregs was assessed by flow cytometry within PBMCs in 2 enrolled patients receiving 20 mg DKY709 daily for the indicated times. “C”: cycle = 4 weeks, “D”: day within cycle, “Pre”: immediately prior to dosing, “Post”: approximately 4 hours post dose.

Supplementary Files

This is a list of supplementary files associated with this preprint. Click to download.

- HeliosDKY709paperSupplementarydatafinal.docx